Edge Detection in Diffusion Weighted MRI Using a Tangent Curve Similarity Metric

Zi'Ang Ding, Xavier Tricoche, and Yaniv Gur

Abstract We present a technique to automatically characterize the geometry of important anatomical structures in diffusion weighted MRI (DWI) data. Our approach is based on the interpretation of diffusion data as a superimposition of multiple line fields that each form a continuum of space filling curves. Using a dense tractography computation, our method quantifies the spatial variations of the geometry of these curves and use the resulting measure to characterize salient structures as edges. Anatomically, these structures have a boundary-like nature and yield a clear picture of major fiber bundles. In particular, the application of our algorithm to high angular resolution imaging (HARDI) data yields a precise geometric description of subtle anatomical configurations associated with the local presence of multiple fiber orientations. We evaluate our technique and study its robustness to noise in the context of a phantom dataset and present results obtained with two diffusion weighted brain images.

1 Introduction

Diffusion weighted imaging (DWI) is a medical imaging technique that measures the anisotropic Brownian motion of water molecules in fibrous tissues and enables their in-vivo investigation. The modeling of the measured multidirectional diffusion information through a second-order tensor, known as diffusion tensor MRI (or DTI), is an important tool for the analysis of the brain's white matter structure [2, 3, 22] and the heart's myocardium [18, 19, 36, 41]. Yet, the gaussian diffusion model used in DTI is unable to adequately model complex diffusion patterns that are common in the white matter such as crossing, fanning, or bent fibers. In such cases, an alternative imaging modality known as high angular resolution diffusion imaging

Z. Ding • X. Tricoche (✉)
Purdue University, West Lafayette, IN, USA
e-mail: ding29@purdue.edu; xmt@purdue.edu

Y. Gur
IBM Research, San Jose, CA, USA
e-mail: guryaniv@us.ibm.com

T. Schultz et al. (eds.), *Modeling, Analysis, and Visualization of Anisotropy*,
Mathematics and Visualization, DOI 10.1007/978-3-319-61358-1_13

(HARDI) proves superior. In HARDI, the measured information is amenable to an orientation distribution function (ODF) that may be described by a higher-order tensor [16, 20, 33] or a band-limited expansion of spherical harmonics [14, 37, 38], which allows one to identify several co-existing significant diffusion directions within a voxel.

Irrespective of the considered diffusion model, the interpretation of the resulting images requires the challenging analysis of a high-dimensional data space. The two main approaches used to facilitate this task are tractography and scalar measures. In tractography one integrates along the dominant diffusion direction(s) to approximate fiber tracts and derive a white matter connectivity map. Both fiber tracts geometry and corresponding connectivity map, in turn, can be used to identify major fiber bundles, which has various clinical applications [39]. The second approach exploits scalar measures derived from the diffusion data, such as fractional anisotropy (FA), or Generalized FA (GFA), for segmentation and analysis [24, 25, 34].

In recent years significant advances in the structural analysis of diffusion tensor fields have been achieved through the extraction of so-called ridge and valley (jointly, *crease*) manifolds from tensor invariants [23, 25]. While crease manifolds have proven successful at characterizing major white matter structures in DTI, no similar investigation was carried out in the context of HARDI problems. Following a different approach, methods considering the end positions of fiber traces in a dense tractogram have been shown to characterize interesting anatomical structures in DTI datasets of the brain's white matter and the heart's myocardium [15, 17].

The approach presented in this paper builds upon a new model of the boundaries of anatomical structures in diffusion weighted MRI as edges of a continuous mapping between spatial locations and the geometric signature of the fiber traces that run through them. By adapting to this geometry-valued setting edge detection techniques devised for scalar images, our method is able to properly characterize subtle anatomical structures in both DTI and HARDI.

Our work advances the state of the art in three significant ways. First, our edge strength measurement is fundamentally nonlocal while prior methods that consider scalar invariants [23, 25] focus on local properties. Second, in contrast to methods that focus on the end points of fiber traces [15, 17], we do not rely on any particular model of curve separation to measure fiber distances and derive a spatial gradient. Third, unlike fiber clustering methods [5, 6, 32], we are not interested in forming bundles from a discrete set of fibers though we are able to explicitly characterize the geometric structures that form the boundaries of fiber bundles.

The main contributions of this paper are

- A novel model that defines structure boundaries as edges of a fiber-valued mapping;
- A tractography-based edge detection method that extracts structures from diffusion weighted MRI;
- A simple conceptual framework applicable both to DTI and HARDI data, that performs well in regions with challenging fiber structures.

The rest of this paper is organized as follows. Section 2 summarizes related work. The details of our edge detection method are provided in Sect. 3 while Sect. 4 presents a number of visualization approaches derived from the measured edge strength to improve the understanding of the anatomical structure information from the DWI signals; Sect. 5 documents the results of our edge detection method on several DWI datasets; and Sect. 6 presents our conclusions and discusses future work.

2 Related Work

We briefly review in the following relevant prior work in DTI and HARDI visualization and analysis.

2.1 Tractography in DTI and HARDI

Tractography is a technique that estimates the trajectories of neural tracts from diffusion weighted MRI data. It provides an effective way to model and analyze the fiber tracts in the white matter, and has further been used to study the structure and connectivity of the human brain [21, 26]. Both in the visualization and medical imaging communities, many methods have been proposed based on the streamline algorithm to perform the tractography in DTI. Assuming the major eigenvector is parallel to the local fiber orientation in each voxel, it is possible to integrate a pathway using numerical integration methods include Euler's method or Runge-Kutta method [4, 8, 31]. Later, several methods using the local diffusion tensor to deflect the incoming direction instead of the major eigenvector are introduced to solve the problem when tracking trough regions of planar anisotropy [27, 47]. Also, streamtubes and streamsurfaces were used to visualize diffusion weighted MRI data [48]. Moreover a MLS-based regularization technique was used to allow tracking to cross noisy regions and gaps [51].

Tracking fibers in higher order tensor (HOT) was first proposed Hlawitschka and Scheuermann as HOT-lines [16]. Schultz and Seidel [33] and Jiao et al. [20] later improved these kind of techniques by introducing tensor decomposition methods to find the local orientations in each step during the integration.

2.2 Diffusion Weighted MRI Analysis

In the medical imaging community, a number of clustering methods which group fiber tracts into anatomical meaningful bundles were used to analyze and investigate information from diffusion weighted MRI. O'Donnell et al. [32] presented a fiber grouping approach that delineates fiber tracts that can be further analyzed for

clinical research purposes. Brun et al. [6] proposed a fiber clustering method to create a weighted undirected graph by comparing fiber tracts pairwise, and perform segmentation in high dimensional space. Also, the same author used laplacian eigenmaps to create a mapping from DTI fiber tracts to a low dimensional Euclidean space, thereby enabling a color coding of fiber tracts that enhances the perception of fiber bundles and connectivity in the human brain [5]. Liang et al. [28] introduced a technique to group fiber tracts into bundles using Nonegative Matrix Factorization (NMF) of the frequency-tract matrix. Mai et al. [30] proposed a method to segment fiber tracts based on a shape similarity measure. To that end they introduced a new technique called Warped Longest Common Subsequence (WLCS), which was used to speed up the segmentation process. Instead of explicitly delineating anatomical structures such as boundaries between fiber bundles, all these fiber clustering methods are interested in organizing a discrete set of fibers into bundles.

In the scientific visualization community, researchers have applied ridge and edge detection methods which were originally developed by computer vision community to the analysis of diffusion weighted MRI data. Kindlmann et al. [23, 25] applied crease surfaces of FA to characterize important anatomical structures in the brain. Extension of this work to ridge lines of FA as models of core lines in fiber bundles was discussed in Tricoche et al. [40]. By defining gradients of shape invariants and rotation tangents [24], Schultz and Seidel successfully extended image processing techniques such as edge detection to diffusion tensor images [34]. However, all these methods focus on local properties and are not able to reveal structures in sub-voxel level.

Also Schultz et al. considered tensor topology [10, 49] in the context of DTI [35] but found the results to lack a clear interpretation. Instead they proposed an alternative topological definition for DTI [35].

In a recent study, a generalized framework for creating super-resolution track-weighed imaging (TWI) was introduced [7]. The intensity of an individual pixel on the resulting image could be determined by a specific property, such as the fractional anisotropy (FA), of the tensorlines which traverse this pixel or the spatial coordinates of those tensorlines.

Most germane to the ideas developed in this paper are recent works applying to tensor field and DTI visualization a technique previously used in flow visualization. Specifically, Hlawitschka et al. [17] and Hlawatsch et al. [15] proposed to use the rate of separation of neighboring fiber tracts as a measure of coherence in DTI volumes. The resulting scalar quantity was able to show certain anatomical structures in human brain and in dog heart.

3 Method

We aim to extract the boundaries of individual fiber bundles as edges of a fiber trace-valued image that we derive from the DWI dataset via dense tractography. First, we wish to motivate some of the choices made in the design of our method by briefly discussing edge detection.

3.1 Edges as Ridges

Edges are fundamental image descriptors in image processing and computer vision and many different techniques have been devised for their extraction [29]. A commonly used approach in that context characterizes edges in a 2-step process: it first computes at each pixel an edge strength measure from which the edge geometry can then be obtained as curves (or surfaces in 3D) along which that edge strength is locally largest.

While edge strength can be measured in scalar images in a variety of ways, we only consider here the simplest possible definition, namely gradient magnitude. Leaving aside for the time being the question of how to robustly compute this gradient, we can see that identifying edges in fiber-valued images necessitates a metric to measure distances, that is dissimilarities between neighboring fibers, which in turn requires the choice of a fiber encoding that lends itself to meaningful distance measures. Once a suitable edge strength has been computed across the dataset, the geometry of the edges can be extracted as ridges of the corresponding field [11].

3.2 Fiber-Valued Image Computation

To create a fiber-valued volume, we first compute a dense, full brain tractogram. The 2nd-order Runge-Kutta method [4] is used to integrate tangent curves along the major eigenvector of the diffusion tensor in DTI datasets. To increase the robustness of our integration, a moving least-squares regularization procedure first proposed by Zhukov and Barr [51, 53] is applied to the tensor field along the integration path. This procedure has the double benefit of increasing the robustness of the integration to the noise inherently present in the data and also to partially mitigate the limitations of the tensor model in regions exhibiting fiber crossing. Indeed, similar to the *tensorline* method [47], the MLS regularization effectively uses the shape of the previously computed filtered tensor value along the curve to constrain the range of directions that the next integration step may take.

Once the integration has been performed, each voxel is assigned an array of 3D positions that describe the geometry of the computed fiber. For the need of subsequent processing, however, a different fiber encoding is needed.

3.3 Feature Encoding

With about a hundred vertices per fiber trace on average, the information associated with each voxel is expressed in a fairly high-dimensional data space. In that space, the straightforward Eulerean metric is both costly to compute and ineffective as dissimilarity measure. Furthermore, the numerical criteria used to control the

progression of the integration (e.g., a lower bound on fractional anisotropy as stop criterion), produce fibers with a varying number of vertices.

To avoid these issues, we map the raw geometric information produced by the fiber tracking step to a low-dimensional representation comprised of the first and second moments of each fiber description [6]. The corresponding set of coefficients f is given in Eq. (1).

$$\mathbf{f} = (m_x, m_y, m_z, h_{xx}, h_{xy}, h_{xz}, h_{yy}, h_{yz}, h_{zz})^\intercal, \tag{1}$$

where $\mathbf{m} = (m_x, m_y, m_z)^\intercal$ is the mean vector of the vertices in 3D space, and the terms $h_{\cdot,\cdot}$ are the independent coefficients of the (symmetric) square root of their covariance matrix $\mathbf{H}$. As a result, each fiber trace is represented by only 9 coefficients that are invariant under flipped fiber orientation. In all datasets we have tested in Sect. 5, this simplification is good enough to capture the geometry of fiber traces. For applications which the first and the second order moment is not enough to distinguish the geometric difference between neighboring fiber traces, any higher order moment could be employed to provide more dimensions in the feature space.

3.4 Edge Strength in Vector-Valued Images

The previous steps of the algorithm yield a volume dataset that associates each data point with a 9D feature vector. To detect edges in this vector-valued image, we need to evaluate its gradient. Our solution consists in computing a linear least squares fit over the 26 neighbors of each voxel. Let f_p denote the feature vector associated with the voxel at position p, the desired linear fit at p is the solution of the following expression:

$$\mathbf{A}_p = \min_{\forall \mathbf{A} \in \mathbb{R}^{9\times 3}} \sum_{q \in N^1(p)} || \mathbf{A}\,(q-p) - \left(\mathbf{f}_q - \mathbf{f}_p\right) ||^2. \tag{2}$$

Here N^1 designates the 1-neighborhood of p, which is comprised of its 26 direct neighbors.

While the corresponding solution $\mathbf{A}_p$ could be used directly as approximation of the gradient $\nabla \mathbf{f}_p$, we adopt in this work a more robust approach. Following prior work on tensor-based feature detection in color images [45], we frame our gradient estimation problem as the construction of a structure tensor on a multichannel volume with 9 parameters. Here, our structure tensor $\mathbf{G}$ is given by

$$\mathbf{G} = \begin{pmatrix} \overline{\mathbf{f}_x^\intercal \mathbf{f}_x} & \overline{\mathbf{f}_x^\intercal \mathbf{f}_y} & \overline{\mathbf{f}_x^\intercal \mathbf{f}_z} \\ \overline{\mathbf{f}_y^\intercal \mathbf{f}_x} & \overline{\mathbf{f}_y^\intercal \mathbf{f}_y} & \overline{\mathbf{f}_y^\intercal \mathbf{f}_z} \\ \overline{\mathbf{f}_z^\intercal \mathbf{f}_x} & \overline{\mathbf{f}_z^\intercal \mathbf{f}_y} & \overline{\mathbf{f}_z^\intercal \mathbf{f}_z} \end{pmatrix}, \tag{3}$$

where the partial derivatives $\mathbf{f}_x$, $\mathbf{f}_y$, and $\mathbf{f}_z$ at p are obtained directly from A_p as its 1st, 2nd, and 3rd columns. The bar $\bar{\cdot}$ indicates the convolution with a Gaussian filter for increased robustness.

Finally, the edge strength s can be measured by a scalar invariant of the structure tensor. Specifically, in our approach, we measure the edge strength as the major eigenvalue of the structure tensor.

$$s = \lambda_{max}(\mathbf{G}) \tag{4}$$

3.5 Extension to HARDI

The DT-MRI model has been shown to fail in regions containing multiple distinct orientations [1, 12, 42]. The HARDI model presented by Tuch et al. [43, 44] extends the single-tensor model to multi-tensor models or ODFs which can capture multiple independent fiber orientations in each voxel, thereby allowing one to track fibers across regions of complex crossing white-matter structures.

In this work, we define the nth higher order tensor which represents the estimated fiber-ODF from DWI signals as follows.

$$\mathbf{D} = \sum_{r=1}^{R} \mathbf{v}_r^1 \otimes \mathbf{v}_r^2 \otimes \cdots \otimes \mathbf{v}_r^n, \tag{5}$$

where $\mathbf{v}$ are vectors and $R = rank(\mathbf{D})$. Further, following prior work we assume that the tensors are supersymmetric, i.e., $\mathbf{v}_r^1 = \mathbf{v}_r^2 = \cdots = \mathbf{v}_r^n$. Unlike the DTI case, the rank of the estimated higher order tensor is unknown. Assuming we are interested in a low-rank approximation of the original higher order tensor, for a given rank $k < R$, $\mathbf{D}$ can be decomposed into k rank-1 tensors.

$$\mathbf{D} \approx \sum_{r=1}^{k} w_r \left(\mathbf{v}_r^1 \otimes \mathbf{v}_r^2 \otimes \cdots \otimes \mathbf{v}_r^n\right), \tag{6}$$

where $\|\mathbf{v}_r\| = 1$, and $\mathbf{v}_r$ represent the possible fiber orientations at the location where $\mathbf{D}$ is estimated. The number k is determined through a simple heuristic method described in [33].

Here we extend our edge detection approach discussed in the DTI Sect. 3.4 to HARDI model and improve the edge detection results by accounting for the presence of multiple orientations in voxels.

For tractography we follow the deterministic higher-order tensor tracking algorithm presented by Hlawitschka and Scheuermann [16] and Schultz and Seidel [33]. More specifically, at each step of the fiber integration, the $rank - k$ decomposition approach is employed to extract the possible fiber orientations from the higher-order

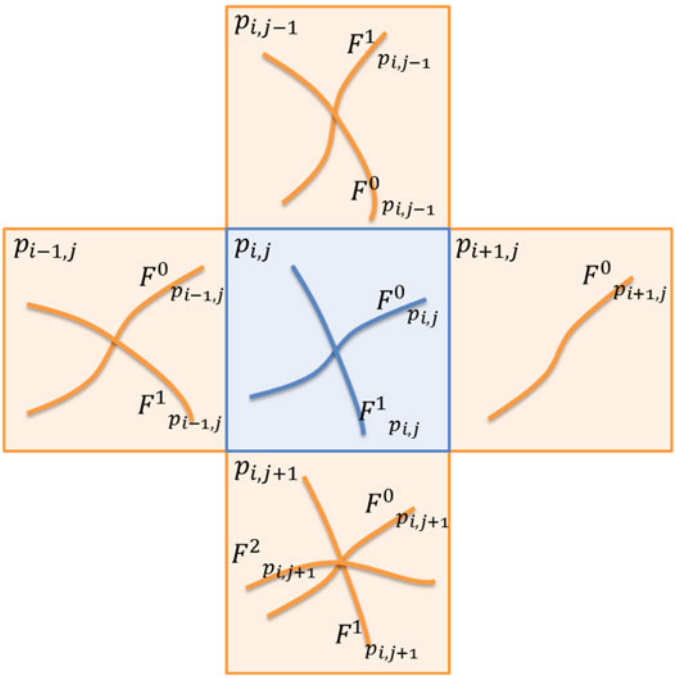

Fig. 1 Case in which neighbor voxels have different number of fibers

tensor. Then an evaluation scheme is applied to find the best orientation, defined as the one forming the smallest angle with the last integration step.

Similar to fiber tracking in DT-MRI, we perform a MLS-based regularization to filter the higher order tensor at each integration step, namely we compute the weighted average of the higher order tensor value within the filter kernel which in this case is defined by the local diffusion ODF.

Unlike DTI, the result of our fiber tracking method on HARDI, for a particular voxel p, could contain M fibers F_p^0, F_p^1, …, F_p^{M-1} corresponding to distinct local orientations $\mathbf{o}_p^0$, $\mathbf{o}_p^1$, …, $\mathbf{o}_p^{M-1}$. Figure 1 illustrates the case in which a different number of fibers is found in voxel $p_{i,j}$ and its neighborhood in 2D.

Since multiple local line fields may coexist, we measure the overall edge strength at a particular voxel p as the sum of individual edge strengths corresponding to fibers F_p^m and their respective local orientation $\mathbf{o}_p^m$. For each possible local orientation $\mathbf{o}_{p_{i,j}}^m$ at voxel $p_{i,j}$ we first construct a local linear fit of feature vectors associated with matching fiber orientations in its neighborhood. Practically, in each surrounding voxel, the fiber with closest orientation to $\mathbf{o}_{p_{i,j}}$ is included in the least squares fit.

As illustrated in Fig. 1, fiber $F_{p_{i-1,j}}^0$, $F_{p_{i+1,j}}^0$, $F_{p_{i,j-1}}^1$, and $F_{p_{i,j+1}}^0$ are selected by fiber $F_{p_{i,j}}^0$ while fiber $F_{p_{i-1,j}}^1$, $F_{p_{i+1,j}}^0$, $F_{p_{i,j-1}}^0$, and $F_{p_{i,j+1}}^1$ are selected by fiber $F_{p_{i,j}}^1$. Note that fiber $F_{p_{i-1,j}}^0$ is selected by both $F_{p_{i,j}}^0$ and $F_{p_{i,j}}^1$, but fiber $F_{p_{i,j+1}}^2$ is never

selected. Applying the above procedure, different fiber functions $\mathbf{f}_p^m$ are estimated from different local fields of space filling curves, then the general derivatives are computed as the mean of derivatives obtained from each $\mathbf{f}_p^m$. As in the DTI case, the structure tensor is employed for a robust estimate of the general derivatives.

$$\mathbf{G} = \sum_{m=0}^{M-1} \begin{pmatrix} \overline{\mathbf{f}_x^{m\top} \mathbf{f}_x^m} & \overline{\mathbf{f}_x^{m\top} \mathbf{f}_y^m} & \overline{\mathbf{f}_x^{m\top} \mathbf{f}_z^m} \\ \overline{\mathbf{f}_y^{m\top} \mathbf{f}_x^m} & \overline{\mathbf{f}_y^{m\top} \mathbf{f}_y^m} & \overline{\mathbf{f}_y^{m\top} \mathbf{f}_z^m} \\ \overline{\mathbf{f}_z^{m\top} \mathbf{f}_x^m} & \overline{\mathbf{f}_z^{m\top} \mathbf{f}_y^m} & \overline{\mathbf{f}_z^{m\top} \mathbf{f}_z^m} \end{pmatrix} \tag{7}$$

Similar to edge detection in DT-MRI, the edge strength is measured by the major eigenvalue of the structure tensor $\mathbf{G}$ in Eq. (4).

4 Visualization

The per voxel edge strength measured by our approach yields a scalar field by applying the measurement to the entire domain of a dataset. Classical scalar field visualization methods, such as isosurfaces and volume rendering are applicable on the edge strength field. However the visualization technique introduced by Hlawitschka et al. [17] which augments the edge strength by overlaying an anisotropy-scaled RGB color map provides the information to identify typical anatomical structures in DWI datasets, the high density of edges detected by our approach could potentially cause visual clutter, especially in the brain dataset. Therefore, in this paper, we split the result visualization into two steps:

1. Characterization of edges' geometry by performing ridge extraction on a user defined sweeping plane or region of interest. The extracted ridge lines/ridge surfaces can further be filtered by the edge strength and ridge strength.
2. Visualizing the ridge lines/ridge surfaces by superimposing an anisotropy-scaled RGB color map which shows the local orientation and fractional anisotropy (FA) to provide the context information of the sweeping plane or the region of interest.

Furthermore, we propose to enhance the visualization result by rendering fiber trajectories with ridge lines/ridge surfaces characterized from our edge strength result (cf. Fig. 8). Hence, the ridge lines/ridge surfaces emphasize the boundary of different anatomical structures while fiber trajectories convey the shape and connectivity of neural tracts.

5 Results and Discussions

Both synthetic and real data were considered to test the presented edge detection approach. First, we focused on a publicly available phantom data to validate our method against a known ground truth and investigate its robustness to various noise levels (Sect. 5.1). Then we studied two human brain datasets (Sects. 5.2 and 5.3).

5.1 Phantom Data

We tested our approach on the phantom data used in the HARDI reconstruction challenge 2013 [9]. The dataset with a $b-value$ of 1200 s/mm^2 and 32 directions was used to test our method on DTI, and the dataset with a $b-value$ of 3000 s/mm^2 and 64 directions was studied to test our method on HARDI. For both DTI and HARDI, two different signal-to-noise-ratio (SNR), 10 and 30, were tested to validate our approach against noise. The original spatial resolution of the phantom is $50 \times 50 \times 50$ with isotropic voxel size as 1.0 mm and we measured the edge strength on a discrete domain with spatial resolution $400 \times 400 \times 400$ in both studies on DTI and HARDI.

Figure 2 shows the edge strength computed from our method both on DTI and HARDI as well as the ground truth. In single orientation regions, both DTI and HARDI can reconstruct the correct orientation, and our approach can successfully detect edges in those regions. In regions which contain crossing fiber tracts from different fiber bundles, DTI leads to incorrect fiber traces. In contrast, the tensor

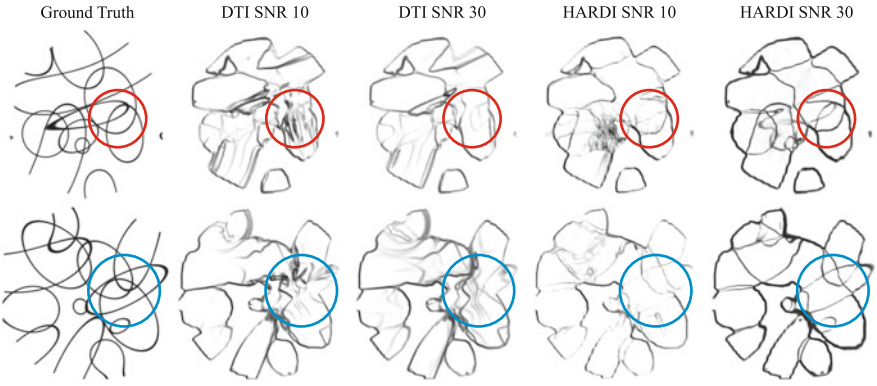

Fig. 2 A comparison of the ground truth and the results obtained by applying our edge detection approach on the phantom dataset with different SNRs. Both *red and blue cycles* highlight the regions where different fiber bundles intersect with each other. It is clear that the edge detection results using DTI fail in those regions. On the other hand, the edge detection results using HARDI delineate meaningful boundaries of fiber bundles similar to the ground truth

decomposition method used in HARDI properly reconstructs the multi-orientation in those regions. Our results in crossing fiber regions shown in Fig. 2 confirm that the DTI results are not close to the ground truth while the HARDI results are comparable to it.

A comparison of our method to the end-position tractography method [15] on DTI is proposed in Fig. 3. Although both methods were implemented with the MLS-based fiber tracking technique [52], the inconsistency of local orientations introduced by DTI model in crossing regions causes incorrect end positions of individual fiber traces. Therefore, using these end positions results a discontinuous

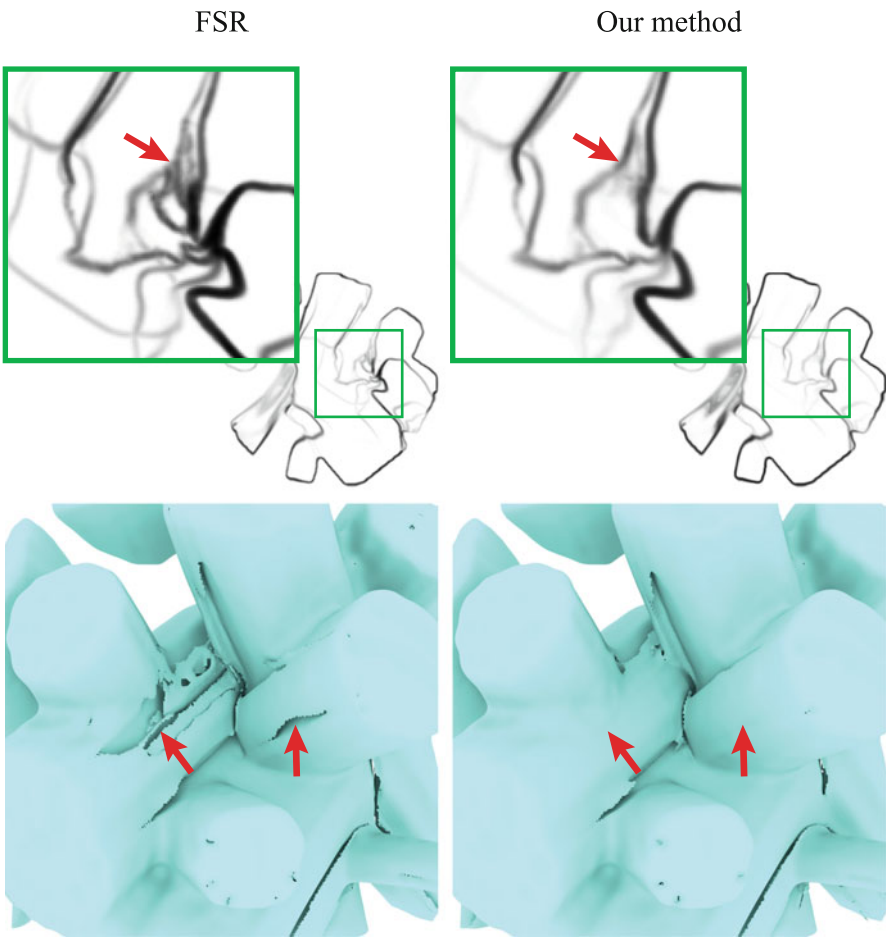

Fig. 3 A detailed comparison of the end-position method and the presented method on phantom dataset. First row visualizes the side-by-side comparison of the edge strength computed from these two methods. Second row shows the ridge surfaces characterized from the edge strength fields. Differences between these two methods are highlighted by *red arrows*

edge strength measurement in FSR. On the other hand, the fiber function estimated by entire fiber traces generates a smooth and consistent result in our approach. The first column shows the edge strength measured by end-position method and our approach on one slice of the YZ plane in the phantom dataset. In single orientation regions, the edge strength measured by our approach is smoother and less influenced by the inconsistency of local orientations caused by noise than the end-position method. The second column shows the characterized ridge surfaces using the same ridge extraction method [13] on edge strength measurement fields generated by end-position method and our approach. Comparing these two ridge surfaces, a significant number of disconnected components and cracks exist in the result of the end-position method.

Finally, the renderings in Fig. 4 show the extracted ridge surfaces from the edge strength on HARDI with SNR = 30 and the boundaries from the ground truth. A unique color was assigned to each fiber bundle, therefore, the correspondence between the characterized ridge surfaces from our edge strength measurement and the actual boundaries of different fiber bundles is clearly shown in these renderings.

5.2 IIT2 Human Brain DTI Template

The first in vivo human brain used to test our approach is the public IIT2 human brain DTI template [50]. The original spatial resolution is $181 \times 217 \times 181$ with isotropic voxel size as 1 mm and the edge strength was measured on a discrete domain with spatial resolution $724 \times 868 \times 724$ which is 4 times larger in each dimension. The relevant fiber tracking parameters are: step-size = 0.1 mm and maximum fiber length = 30.0 mm. The stopping criteria in fiber tracking are set as the maximum angle between steps = 45° and the FA value threshold for white matter = 0.15.

Ridge surfaces rendered as Fig. 5a and b are extracted from the edge strength measured by our edge detection approach in the brainstem (the posterior part of the brain). Complex fiber traces with distinct directions pass through this region. Similar to (f) which is taken from Fig. 5 in Kindlmann et al. [25], boundaries of different fiber traces including the *middle cerebellar peduncle* (mcp), *corticospinal tract*(cst), *transverse pontine fibers* (tpf), *medial lemniscus* (ml), *superior cerebellar peduncle* (scp), and *inferior cerebellar peduncle* (icp) are identified and visualized with the difference that our results exhibit more comprehensive and clear boundaries. In addition, two images (d) and (e) visualize the characterized ridge lines corresponding to the cutting plane *i* and *ii* in (c).

The yellow cycle in Fig. 6a indicates another interesting region where the white matter lateral to the posterior horn of the lateral ventricle consists of three layers of tracts: the most lateral layer is the *superior longitudinal fasciulus* (slf) with a superior-inferior orientation; the most medial layer is the callosal projection to the *temporal lobe* (tapetum); and the *posterior region of the corona radiata* (pcr) can be found between them with an anterior-posterior orientation [46]. Boundaries between

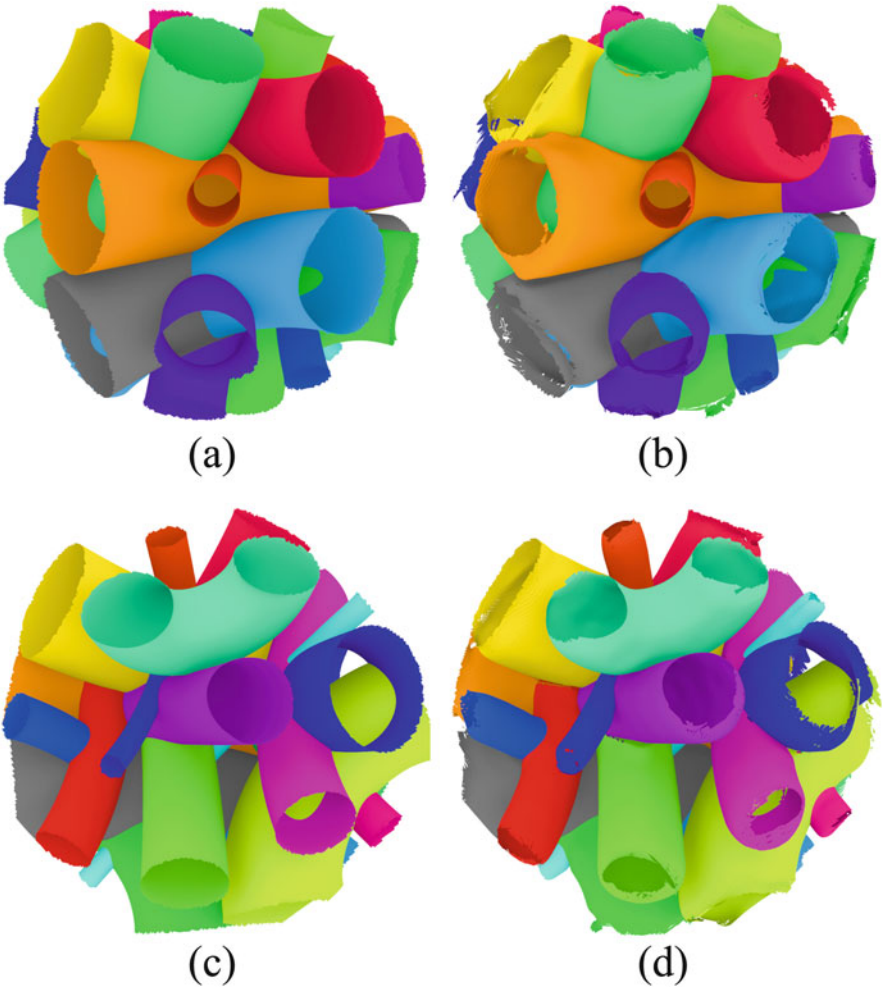

Fig. 4 Ridge surfaces characterized from the edge strength measured on HARDI with SNR=30. (**a**) and (**c**) boundaries of different fiber bundles from the ground truth. (**b**) and (**d**) extracted ridge surfaces by our approach

these three layers are successfully detected by our approach as shown in Fig. 6b. Figure 6c shows the ridge surfaces extracted from our edge strength measurement. A visualization which overlays the anisotropy-based RGB color map with ridge surfaces is shown in Fig. 6d. This result confirms that the detected edges do represent the actual boundaries between different white matter layers.

Figure 7a highlightes 9 anatomical structures on a anisotropy-based RGB color map of a coronal plane. Figure 7b and c visualize edge strength measured with 2 times and 4 times as large as the original spatial resolution in each dimension respectively. It takes about 5 s to measure the edge strength of Fig. 7b and 13 s of

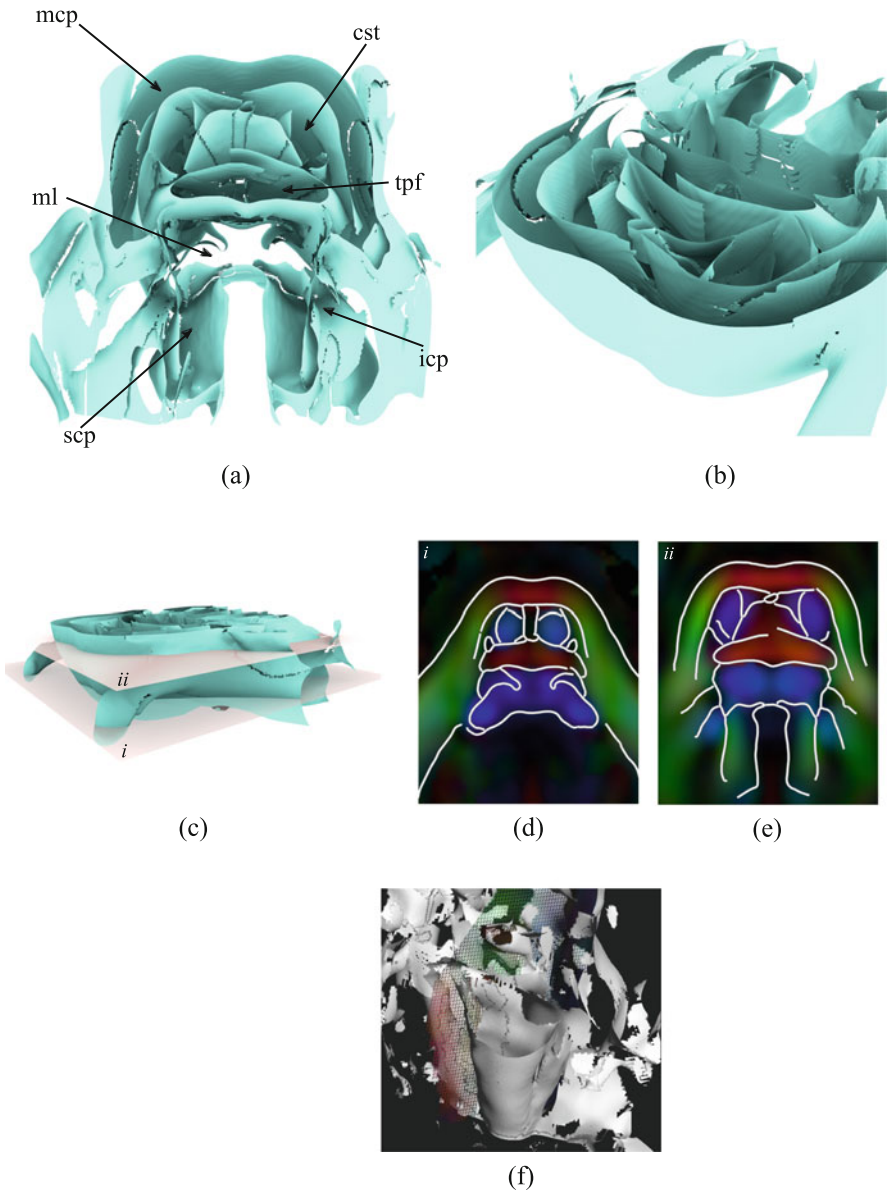

Fig. 5 Edge detection result in the brainstem by our approach. mcp: middle cerebellar peduncle; cst: corticospinal tract; tpf: transverse pontine fibers; ml: medial lemniscus; scp: superior cerebellar peduncle; icp: inferior cerebellar peduncle.

Fig. 7c on a machine with an Intel i7 quad-core CPU and a Nvidia Quadro M3000M graphics card. In general, the edge strength measured with a higher resolution

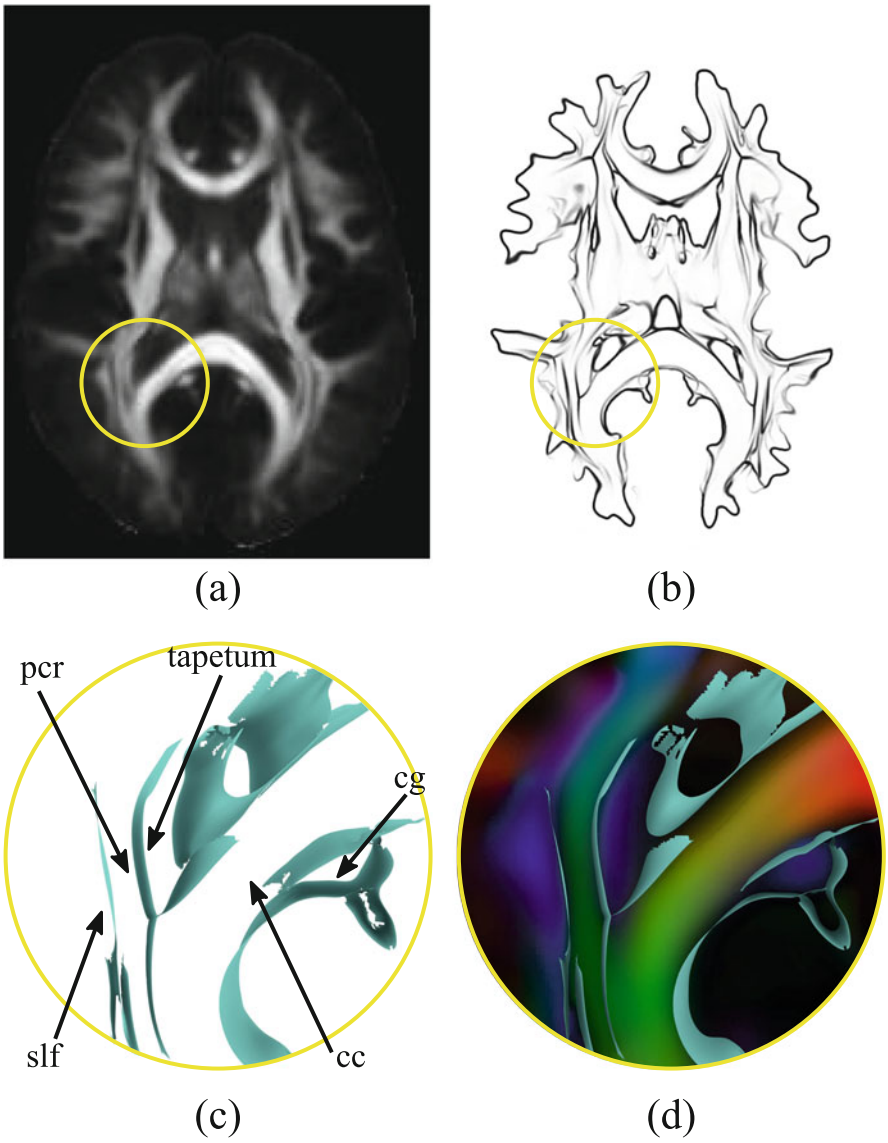

Fig. 6 Edge detection results in an interesting region where the white matter lateral to the posterior horn of the lateral ventricle consists of three layers of tracts. cc: corpus callosum; cg: cingulum; pcr: posterior region of corona radiata; slf: superior longitudinal fasciculus. (**a**) Fractional anisotropy (FA) of the brain white matter visualized on a transverse section. The *circle* indicates the considered anatomical region. (**b**) Edge strength measured by our method on the same section. (**c**) Ridge surfaces of the edge strength characterize the complex geometry of crossing fibers in the area of interest. (**d**) Same as (**c**) with FA overlaid and color-coded by the orientation of the main diffusion direction

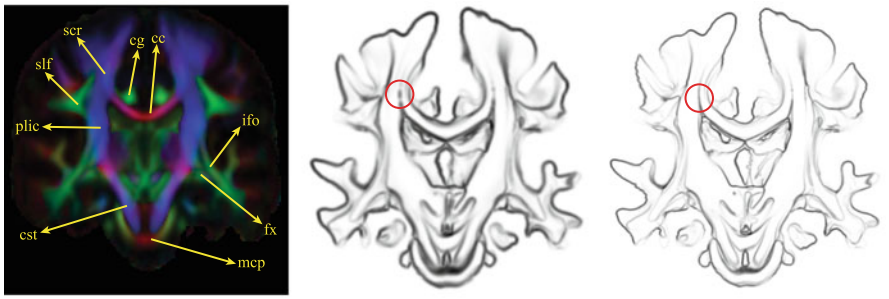

Fig. 7 (**a**) Coronal anisotropy-based RGB color map; (**b**) edge strength measured with 2 times as large as the original spatial resolution in each dimension; (**c**) edge strength measured with 4 times as large as the original spatial resolution in each dimension. cc: *corpus callosum*; cg: *cingulum*; st: *corticospinal tract*; mcp: *middle cerebellar peduncle*; fx: *fornix*; ifo: *inferior fronto-occipital fasciculus*; plic: *posterior limb of internal capsule*; scr: *superior region of internal capsule*; slf: *superior longitudinal fasciculus*

exhibits sharper edges and contains less discontinuity than the one measured with a lower resolution. However, both results are able to capture the boundaries of anatomical structures highlighted in Fig. 7a.

5.3 Human Brain with DTI and HARDI

The second in vivo human brain dataset used to test our approach consists of 270 diffusion weighted images with three different $b-values$, 1000 s/mm^2, 2000 s/mm^2, and 3000 s/mm^2, as well as 18 baseline scans with $b-value = 0$. Multiple $b-value$ allows us to test our method on DTI and HARDI separately and compare the results. We use the diffusion weighted images with $b - value = 1000$ s/mm^2 to estimate a DTI dataset, and use the ones with $b - value = 3000$ s/mm^2 to estimate a HARDI dataset.

In this experiment, a small region of interest was selected where the lateral *transcallosal fibers* (tf) runs through the *corpus callosum* (cc) and intersects with the *internal capsule* (ic). The DTI model yields invalid orientation information in the fiber crossing region while HARDI successfully reconstructs the *transcallosal fibers*. Our edge detection approach on HARDI could extract edges that correctly represent the anatomical structures in this region. A side-by-side comparison of our edge detection results on DTI and HARDI is shown in Fig. 8. Figure 8 also highlights the anatomical structures that could be found by our approach both on DTI and HARDI with corresponding fiber traces. As can be seen, both DTI and HARDI allowed our method capture boundaries of *corpus callosum* (red) and *cingulum* (green), while it was only in the HARDI case that our method succeeded in reconstructing the boundaries of *transcallosal fibers* (purple). Similarly, the crossing

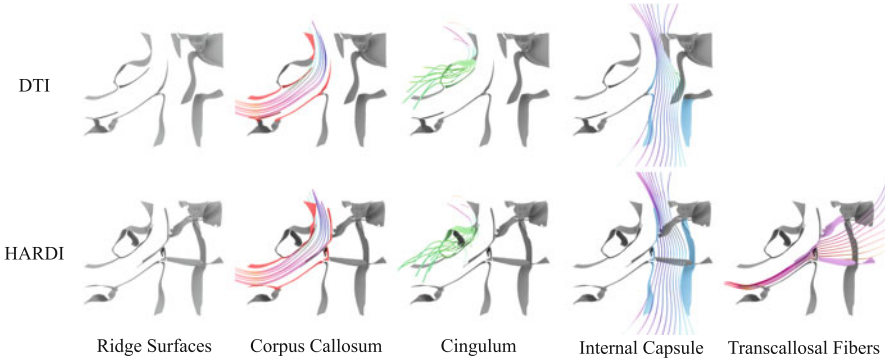

Fig. 8 A comparison of the ridge surfaces extracted from the edge detection results by our approach on DTI and HARDI

of *internal capsule* and *superior longitudinal fasciculus* (blue) was not properly characterized in DTI data, which led to the partial extraction of the boundaries of the *internal capsule* (blue) in this case. In contrast, edge extraction in the HARDI case produces correct boundaries between *internal capsule* and *superior longitudinal fasciculus*.

6 Conclusion and Future Work

In many applications of diffusion weighted imaging (DWI) analysis, extracting the boundaries of anatomical structures from the scanned DWI signals is a crucial step. In this paper, we have presented an tractography-based edge detection technique for DWI that takes the entire geometry of fiber traces into consideration to identify the contour of distinct fiber populations. An evaluation against ground truth in a phantom dataset has proved that the edges characterized by our method coincide with the boundaries of individual fiber bundles and thereby reveal major anatomical structures. In addition, experiments performed on real data have shown that subtle anatomical structures, in particular those associated with fiber crossings, can be identified by our method in noisy datasets.

Limitations of our approach and open questions remain as avenues for future work. First, the super-sampling of the original dataset combined with an on-the-fly regularization procedure at each step of fiber integration make our technique computationally expensive. Although a GPU implementation was used to accelerate the necessary computations, a strategy consisting in reusing fiber traces among neighboring voxels could dramatically reduce the computational time by exploiting redundancy. Second, standard tensor invariant information like fractional anisotropy (FA) aggregated along individual fiber traces could also be used to measure edge strength in the context of Diffusion Tensor Imaging. Finally, the basic approach

presented in this paper is not limited to the visualization of DWI data, and we would like to apply it to tensor field visualization problems in other application domains.

Acknowledgements This work was made possible in part by a NSF CAREER Program Award No. 1150000: Efficient Structural Analysis of Multivariate Fields for Scalable Visualizations. This support is here gratefully acknowledged.

References

1. Alexander, D.C., Barker, G.J., Arridge, S.R.: Detection and modeling of non-Gaussian apparent diffusion coefficient profiles in human brain data. Magn. Reson. Med. **48**(2), 331–340 (2002)
2. Basser, P.J., Pierpaoli, C.: Microstructural and physiological features of tissues elucidated by quantitative-diffusion-tensor MRI. J. Mag. Reson. Ser. B **111**(3), 209–219 (1996)
3. Basser, P.J., Mattiello, J., LeBihan, D.: MR diffusion tensor spectroscopy and imaging. Biophys. J. **66**(1), 259–267 (1994)
4. Basser, P.J., Pajevic, S., Pierpaoli, C., Duda, J., Aldroubi, A.: In vivo fiber tractography using DT-MRI data. Magn. Reson. Med. **44**(4), 625–32 (2000)
5. Brun, A., Park, H.-J., Knutsson, H., Westin, C.-F.: Coloring of DT-MRI fiber traces using laplacian eigenmaps. In: Diaz, R.M., Arencibia, A.Q. (eds.) Computer Aided Systems Theory (EUROCAST'03). Lecture Notes in Computer Science 2809, pp. 564–572, Las Palmas de Gran Canaria, Spain, 24–28 Feb 2003. Springer, Berlin (2003)
6. Brun, A., Knutsson, H., Park, H.J., Shenton, M.E., Westin, C.-F.: Clustering fiber tracts using normalized cuts. In: *Seventh International Conference on Medical Image Computing and Computer-Assisted Intervention (MICCAI'04)*. Lecture Notes in Computer Science, pp. 368–375, Rennes – Saint Malo, France, Sept 2004
7. Calamante, F., Tournier, J.-D., Smith, R.E., Connelly, A.: A generalised framework for super-resolution track-weighted imaging. NeuroImage **59**(3), 2494–2503 (2012)
8. Conturo, T.E., Lori, N.F., Cull, T.S., Akbudak, E., Snyder, A.Z., Shimony, J.S., McKinstry, R.C., Burton, H., Raichle, M.E.: Tracking neuronal fiber pathways in the living human brain. Proc. Natl. Acad. Sci. **96**(18), 10422–10427 (1999)
9. Daducci, A., Caruyer, E., Descoteaux, M., Houde, J.-C., Thiran, J.-P.: Hardi reconstruction challenge. In: IEEE ISBI (2013)
10. Delmarcelle, T., Hesselink, L.: The topology of symmetric, second-order tensor fields. In: Proceedings of IEEE Visualization 1994, pp. 140–147. IEEE Computer Society Press, Los Alamitos, CA (1994)
11. Eberly, D.: Ridges in Image and Data Analysis. Kluwer Academic Publishers, Boston (1996)
12. Frank, L.R.: Characterization of anisotropy in high angular resolution diffusion-weighted MRI. Magn. Reson. Med **47**, 1083–1099 (2002)
13. Furst, J.D., Pizer, S.M.: Marching ridges. In: Signal and Image Processing, pp. 22–26 (2001)
14. Hess, C.P., Mukherjee, P., Han, E.T., Xu, D., Vigneron, D.B.: Q-ball reconstruction of multimodal fiber orientations using the spherical harmonic basis. Magn. Reson. Med. **56**(1), 104–117 (2006)
15. Hlawatsch, M., Vollrath, J.E., Sadlo, F., Weiskopf, D.: Coherent structures of characteristic curves in symmetric second order tensor fields. IEEE Trans. Vis. Comput. Graph. **17**(6), 781–794 (2011)
16. Hlawitschka, M., Scheuermann, G.: Hot-lines: tracking lines in higher order tensor fields. In: IEEE Visualization, 2005. VIS 05, pp. 27–34, Oct. 2005
17. Hlawitschka, M., Garth, C., Tricoche, X., Kindlmann, G., Scheuermann, G., Joy, K.I., Hamann, B.: Direct visualization of fiber information by coherence. Int. J. Comput. Assist. Radiol. Surg. **5**(2), 125–131 (2010)

18. Holmes, A.A., Scollan, D.F., Winslow, R.L.: Direct histological validation of diffusion tensor MRI in formaldehyde-fixed myocardium. Magn. Reson. Med. **44**(1), 157–61 (2000)
19. Hsu, E.W., Muzikant, A.L., Matulevicius, S.A., Penland, R.C., Henriquez, C.S.: Magnetic resonance myocardial fiber-orientation mapping with direct histological correlation. Am. J. Physiol. **274**(5 Pt 2), H1627–1634 (1998). 0002-9513 (Print) Journal Article Research Support, U.S. Gov't, Non-P.H.S. Research Support, U.S. Gov't, P.H.S.
20. Jiao, F., Gur, Y., Johnson, C.R., Joshi, S.: Detection of crossing white matter fibers with high-order tensors and rank-k decompositions. In: Information Processing in Medical Imaging, pp. 538–549. Springer, London (2011)
21. Jones, D.K.: Studying connections in the living human brain with diffusion MRI. Cortex **44**(8), 936–952 (2008)
22. Jones, D.K., Simmons, A., Williams, S.C.R., Horsfield, M.A.: Non-invasive assessment of axonal fiber connectivity in the human brain via diffusion tensor MRI. Magn. Reson. Med. **42**(1), 37–41 (1999)
23. Kindlmann, G., Tricoche, X., Westin, C.-F.: Anisotropy creases delineate white matter structure in diffusion tensor MRI. In: Proceedings of Medical Imaging Computing and Computer-Assisted Intervention, MICCAI '06 (2006)
24. Kindlmann, G., Ennis, D.B., Whitaker, R.T., Westin, C.-F.: Diffusion tensor analysis with invariant gradients and rotation tangents. IEEE Trans. Med. Imaging **26**(11), 1483–1499 (2007)
25. Kindlmann, G., Tricoche, X., Westin, C.-F.: Delineating white matter structure in diffusion tensor MRI with anisotropy creases. Med. Image Anal. **11**(5), 492–502 (2007)
26. Lazar, M.: Mapping brain anatomical connectivity using white matter tractography. NMR in Biomed. **23**(7), 821–835 (2010)
27. Lazar, M., Weinstein, D.M., Tsuruda, J.S., Hasan, K.M., Arfanakis, K., Meyerand, M.E., Badie, B., Rowley, H.A., Haughton, V., Field, A., et al.: White matter tractography using diffusion tensor deflection. Hum. Brain Mapp. **18**(4), 306–321 (2003)
28. Liang, X., Wang, J., Lin, Z., Zhang, C.: White matter fiber tract segmentation using nonnegative matrix factorization. In: 3rd International Conference on Bioinformatics and Biomedical Engineering, 2009. ICBBE 2009, pp. 1–4 (2009)
29. Lindeberg, T.: Edge detection and ridge detection with automatic scale selection. Int. J. Comput. Vis. **30**(2), 77–116 (1998)
30. Mai, S.T., Goebl, S., Plant, C.: A similarity model and segmentation algorithm for white matter fiber tracts. In: 2012 IEEE 12th International Conference on Data Mining (ICDM), pp. 1014–1019 (2012)
31. Mori, S., Crain, B.J., Chacko, V.P., Van Zijl, P.: Three-dimensional tracking of axonal projections in the brain by magnetic resonance imaging. Ann. Neurol. **45**(2), 265–269 (1999)
32. O'Donnell, L., Kubicki, M., Shenton, M.E., Dreusicke, M., Grimson, W.E.L., Westin, C.-F.: A method for clustering white matter fiber tracts. AJNR Am. J. Neuroradiol. **27**(5), 1032–1036 (2006)
33. Schultz, T., Seidel, H.-P.: Estimating crossing fibers: a tensor decomposition approach. IEEE Trans. Vis. Comput. Graph. (Proc. IEEE Vis.) **14**(6), 1635–1642 (2008)
34. Schultz, T., Seidel, H.-P.: Using eigenvalue derivatives for edge detection in DT-MRI data. In: Rigoll, G. (ed.) Pattern Recognition. Lecture Notes in Computer Science, vol. 5096, pp. 193–202. Springer, New York (2008)
35. Schultz, T., Theisel, H., Seidel, H.-P.: Topological visualization of brain diffusion MRI data. IEEE Trans. Vis. Comput. Graph. (Proc. IEEE Vis.) **13**(6), 1496–1503 (2007)
36. Scollan, D.F., Holmes, A., Winslow, R., Forder, J.: Histological validation of myocardial microstructure obtained from diffusion tensor magnetic resonance imaging. Am. J. Physiol. **275**, 2308–2318 (1998)
37. Tournier, J.-D., Calamante, F., Gadian, D.G., Connelly, A.: Direct estimation of the fiber orientation density function from diffusion-weighted MRI data using spherical deconvolution. NeuroImage **23**, 1176–1185 (2004)
38. Tournier, J.-D., Calamante, F., Connelly, A.: Robust determination of the fibre orientation distribution in diffusion MRI: non-negativity constrained super-resolved spherical deconvolution. NeuroImage **35**, 1459–1472 (2007)

39. Travers, B.G., Adluru, N., Ennis, C., Tromp, D.P.M., Destiche, D., Doran, S., Bigler, E.D., Lange, N., Lainhart, J.E., Alexander, A.L.: Diffusion tensor imaging in autism spectrum disorder: a review. Autism Res. **5**(5), 289–313 (2012)
40. Tricoche, X., Kindlmann, G., Westin, C.-F.: Invariant crease lines for topological and structural analysis of tensor fields. IEEE Trans. Vis. Comput. Graph. **14**(6), 1627–1634 (2008)
41. Tseng, W.-Y.I., Wedeen, V.J., Reese, T.G., Smith, R.N., Halpern, E.F.: Diffusion tensor MRI of myocardial fibers and sheets: correspondence with visible cut-face texture. J. Mag. Reson. Imaging **17**(1), 31–42 (2003)
42. Tuch, D.S.: Diffusion MRI of complex tissue structure. PhD thesis, Massachusetts Institute of Technology, Cambridge, MA, Jan 2002
43. Tuch, D.S., Weisskoff, R.M., Belliveau, J.W., Wedeen, V.J.: Clustering fiber tracts using normalized cuts. In: Proceeding of the 7th Anmual Meeting of ISMRM, p. 321, Philadephia, PA, 1999
44. Tuch, D.S., Reese, T.G., Wiegell, M.R., Wedeen, V.J.: Diffusion MRI of complex neural architecture. Neuron **40**, 885–895 (2003)
45. van de Weijer, J., Gevers, Th.: Tensor based feature detection for color images. In: Color and Imaging Conference, vol. 2004, no. 1, pp. 100–105. Society for Imaging Science and Technology (2004)
46. Wakana, S., Jiang, H., Nagae-Poetscher, L.M., Van Zijl, P.C.M., Mori, S.: Fiber tract–based atlas of human white matter anatomy 1. Radiology **230**(1), 77–87 (2004)
47. Weinstein, D., Kindlmann, G., Lundberg, E.: Tensorlines: advection-diffusion based propagation through diffusion tensor fields. In: Proceedings of the Conference on Visualization'99: Celebrating Ten Years, pp. 249–253. IEEE Computer Society Press, Los Alamitos, CA (1999)
48. Zhang, S., Demiralp, C., Laidlaw, D.H.: Visualizing diffusion tensor MR images using streamtubes and streamsurfaces. IEEE Trans. Vis. Comput. Graph. **9**(4), 454–462 (2003)
49. Zheng, X., Parlett, B.N., Pang, A.: Topological lines in 3D tensor fields and discriminant hessian factorization. IEEE Trans. Vis. Comput. Graph. **11**(4), 395–407 (2005)
50. Zhang, S., Peng, H., Dawe, R.J., Arfanakis, K.: Enhanced icbm diffusion tensor template of the human brain. Neuroimage **54**(2), 974–984 (2011)
51. Zhukov, L., Barr, A.: Oriented tensor reconstruction: tracing neural pathways from diffusion tensor MRI. In: Proceedings of IEEE Visualization 2002, pp. 387–394 (2002)
52. Zhukov, L., Barr, A.H.: Oriented tensor reconstruction: tracing neural pathways from diffusion tensor MRI. In: IEEE Visualization, 2002. VIS 2002, pp. 387–394. IEEE, Piscataway, NJ (2002)
53. Zhukov, L., Barr, A.: Heart -muscle fiber reconstruction from diffusion tensor MRI. In: Proceedings of IEEE Visualization 2003, pp. 597–602 (2003)